JOURNAL OF GEOPHYSICAL RESEARCH, VOL. 115, D12113, doi:10.1029/2009JD012431, 2010

Multidecadal CO_2 uptake variability of the North Atlantic

Ulrike Löptien[1,2] and Carsten Eden[1]

Received 5 May 2009; revised 4 February 2010; accepted 17 February 2010; published 22 June 2010.

[1] The multidecadal variability of air-sea CO_2 fluxes in the North Atlantic under preindustrial atmospheric CO_2 conditions is simulated, using a coupled biogeochemical/circulation model driven by long-term surface forcing reconstructed from the leading modes of sea level pressure observations from 1850 to 2000. Heat fluxes are of great importance for the multidecadal CO_2 fluctuations, about equal in magnitude to wind stress, in contrast to their less prominent role for CO_2 flux variability on interannual timescales. Another difference, compared to higher frequencies, is the dominance of the North Atlantic Oscillation in driving the variability of the air-sea CO_2 fluxes. Two spatially distinct regimes lead to large anomalies in the CO_2 fluxes but compensate to a large degree. The first regime is advective and has its clear signature southeast of Greenland while the second one, in the vicinity of the Labrador Sea and off Newfoundland, is convective. In both regimes, the multidecadal CO_2 fluctuations are driven mainly by variations in temperature, salinity, and DIC content at the sea surface while the role of the biological pump is of minor importance in this particular model. The magnitude of the simulated multidecadal CO_2 uptake changes is on the order of 0.02 Pg C/yr and amounts to 10–15% of the estimated annual anthropogenic CO_2 uptake of the North Atlantic.

Citation: Löptien, U., and C. Eden (2010), Multidecadal CO_2 uptake variability of the North Atlantic, *J. Geophys. Res.*, *115*, D12113, doi:10.1029/2009JD012431.

1. Introduction

[2] The ocean and the terrestrial ecosystems are large sinks for CO_2, such that at present, less than half of the anthropogenic CO_2 emissions remain in the atmosphere. In order to estimate the possible effects of future CO_2 emissions the capacity and the sensitivity to climate change of these sinks has to be understood in detail. The natural variability of CO_2 uptake is one factor of uncertainty when estimating the future uptake of anthropogenic CO_2 by the oceans. While direct global observational estimates of interannual air-sea CO_2 flux variability are difficult to obtain, ocean models offer a possibility to infer such information indirectly. Numerous studies exist for the world ocean: *LeQuere et al.* [2000] estimated in a "robust diagnostic" ocean circulation model natural interannual variability of the air-sea CO_2 flux of ±0.4 Pg C/yr (a model in which the flow field remains inconsistent with the simulated temperature and salinity distribution which are forced to observations by artificial source terms.) *Obata and Kitamura* [2003] and *Wetzel et al.* [2005] simulated with fully prognostic global ocean models a standard deviation of interannual oceanic CO_2 uptake variability of 0.23 Pg C/yr and 0.25 Pg C/yr over the last 50 years, respectively.

[3] Ocean model simulations have demonstrated that the tropical Pacific plays the largest role for the interannual CO_2 flux variability while the role of the North Atlantic causes still some discussion [*McKinley et al.*, 2004]. Although the North Atlantic takes up a large fraction of anthropogenic CO_2 [*Sabine et al.*, 2004], most carbon cycle simulations agree in the finding that interannual flux variability in the North Atlantic does not contribute significantly to the interannual global CO_2 flux variability. A recent study of *Watson et al.* [2009] reports, however, substantial variations in the annual fluxes by more than a factor of two. Those estimates are derived from annual flux estimates obtained by VOS observations between northwestern Europe and the Caribbean (2002–2007). Also, the analysis of a time series of CO_2 flux estimates at Bermuda by *Gruber et al.* [2002] suggests that basin-scale flux pattern related to the NAO might force interannual CO_2 flux variability in the North Atlantic as large as 0.3 Pg C/yr. *McKinley et al.* [2004] argued, based on their model simulation, that the local time series at Bermuda may not be representative for the CO_2 uptake variability of the whole North Atlantic, such that no significant correlations could be found between NAO and CO_2 uptake by the North Atlantic. *Raynaud et al.* [2005] found in an ocean model simulation the cancelation of interannual CO_2 flux anomalies of different sign over different parts of the North Atlantic. This explains the low relative importance of the North Atlantic for global CO_2 flux variability and the low correlation of the interannual CO_2 uptake of the North Atlantic with the NAO.

[4] Since the availability of the surface flux data from reanalysis data products or other origin which could be used

[1]Leibniz Institute of Marine Sciences at University of Kiel (IFM-GEOMAR), Kiel, Germany.
[2]Now at Swedish Meteorological and Hydrological Institute, Norrköping, Sweden.

0148-0227/10/2009JD012431

to force ocean models is limited to roughly 50 years, all model studies referenced above focus mainly on interannual to decadal variability in CO_2 flux variability. To extend such ocean model simulations, we reconstruct the surface forcing for the last 150 years using long-term sea level pressure data following the method of *Eden and Jung* [2001] who reproduced observed multidecadal SST anomalies and implied circulation changes. For computational and conceptional simplicity, the atmospheric CO_2 concentration is set to a constant preindustrial level. Thus, our study focuses on the variability of the CO_2 uptake neglecting the anthropogenic effect apart from the indirect inclusion through atmospheric heat fluxes and wind stress. Given the apparent absence of strong nonlinear responses of the ocean to the steady rise of atmospheric (up to now) our conclusions about the decadal variability can be assumed to remain valid when anthropogenic CO_2 is considered.

2. Model and Methods

2.1. Model Configuration

[5] The present study is based on integrations of a non-eddy-resolving regional model of the North Atlantic. The numerical code is a rewritten version of the GFDL MOM2.1 code [*Pacanowski*, 1995] and can be found at http://www.ifm-geomar.de/~spflame. The model domain ranges from 70°N to 18°S and 100°W to 30°E with closed boundaries in the north and south and in the Strait of Gibraltar, where we use restoring zones for temperature, salinity and the biogeochemical tracers. The horizontal resolution is 4/3° in longitude and 4/3° cos ϕ in latitude (ϕ). The vertical grid has 45 vertical levels with thickness ranging from 10 m near the surface to 250 m at the deepest level of 5500 m. Unresolved subgrid-scale processes are parameterized by harmonic diffusion and friction terms. Temperature and salinity are mixed along neutral surfaces after *Cox* [1987] and by the eddy-induced tracer advection parameterization of *Gent and McWilliams* [1990]. Model parameters are chosen as described by *Eden and Jung* [2001], except for changes in the different mixed layer parameterization which is now formulated after *Gaspar et al.* [1990].

[6] The model was driven by climatological monthly mean forcing in a 100 year spin-up period to allow for a dynamical adjustment of the circulation. Sea surface salinity was restored toward climatological values during the first 50 years of the spin-up. Afterward the model was driven by the diagnosed freshwater fluxes fields from the year 50. The switch from the restoring boundary conditions to the fixed diagnosed freshwater flux induces only a small model drift in the subsequent integration over 200 years and is necessary due to the lack of balanced surface freshwater fluxes from observational estimates. The surface heat flux forcing is formulated as a Haney-type surface boundary condition [*Haney*, 1971] (i.e., a restoring term is added to the heat flux formulation). The spatially and monthly varying restoring coefficient was determined from a linearization of net heat bulk formulas. The surface heat flux formulation and the climatological wind stress were derived from an analysis of the ECMWF weather forecast model [*Barnier et al.*, 1995]. As a simple parameterization of sea ice, surface cooling, freshwater fluxes and fluxes of turbulent kinetic energy are set to zero when the SST is at or bellow the freezing point.

[7] After the first 100 year spin-up period the circulation model was coupled to a nitrogen-based pelagic ecosystem model and was integrated for another 50 years, allowing for an adjustment of the biogeochemical variables within the main thermocline. The ecosystem model consists of four compartments, namely nitrate, phytoplankton, zooplankton and detritus (a so-called NPZD model) and is described in more detail by *Oschlies and Garcon* [1999] and *Eden and Oschlies* [2006]. This ecosystem model is coupled to a compartment of dissolved inorganic carbon (DIC) using a carbon (C) to nitrate (N) ratio of C/N = 6.6. Denitrification is not included in the model. Initial conditions and boundary conditions for nitrate are taken from *Boyer and Levitus* [1997] and for DIC from the observational estimate of preindustrial DIC from GLODAP [*Sabine et al.*, 2004] while the initial conditions for phytoplankton, zooplankton and detritus are set to small nonnegative values.

[8] In contrast to the compartments of the NPZD model, the distribution of DIC is affected by air sea fluxes. The formulation of air-sea gas exchange follows *Wanninkhof* [1992] and the atmospheric CO_2 concentration was set to the mean preindustrial value of 278 ppm varying with season and latitude following a nonlinear fit to observational estimates by *Conway et al.* [1994]. The partial pressure of CO_2 in the ocean is calculated from total alkalinity, DIC, temperature, salinity and atmospheric sea level pressure following OCMIP standards. Contributions by variable nitrate, silicate, phosphate, etc. concentrations on pH are neglected. Since alkalinity is not a prognostic variable, we use a nonlinear empirical fit of surface salinity versus alkalinity for the North Atlantic domain. A more detailed description is given by *Eden and Oschlies* [2006].

2.2. Reconstructing Multidecadal Forcing

[9] After the spin-up phase, monthly mean surface flux anomalies were added to the climatological surface forcing to drive the model in a 150 year hindcast simulation. Note that reanalysis data sets, as usually used for such ocean hindcast simulation, reach back to 1948 at most. To overcome this limitation in the availability of surface flux data for multidecadal ocean model simulations, we reconstruct the surface fluxes for the period 1850–2000 using leading modes of long-term sea level pressure data.

[10] First, we perform a standard EOF analysis for the monthly mean sea level pressure (SLP) of the North Atlantic sector of the NCEP/NCAR reanalysis data [*Kalnay et al.*, 1996]. The result of such an EOF analysis is discussed, e.g., by *Cayan* [1992]. The leading EOF shows a dipole structure over the North Atlantic and the corresponding time series (PC) resembles closely the NAO index. The PCs of the SLP are then regressed on the monthly mean surface heat fluxes and wind stress time series from the NCEP/NCAR data, which yield a regression pattern for each PC in surface heat flux and wind stress. These patterns describe the interannual variability in surface heat flux and wind stress connected to the individual EOF of the SLP. The resulting pattern for the leading EOF shows for instance the familiar tripolar structure for the wintertime surface heat fluxes and enhanced westerly wind stress in the North Atlantic [*Cayan*, 1992; *Hurrell et al.*, 2003].

Table 1. Acronyms for Model Experiments[a]

Experiment	PCs[b]	Heat Flux	Wind Stress
NAO-FULL	1	yes	Yes
NAO-WIND	1	no	Yes
NAO-HEAT	1	yes	No
2PC-FULL	2	yes	Yes
4PC-FULL	4	yes	Yes
NCEP-FULL[c]	-	yes	Yes

[a]In all experiments the model is driven by either interannual variability in surface heat flux, wind stress, or both.
[b]Denotes the number of PCs of SLP from NCEP/NCAR used for reconstruction of the surface forcing.
[c]In experiment NCEP-FULL, the model was driven by the unmodified surface forcing function from NCEP/NCAR data set.

[11] Next we regress the first *n* leading EOFs of SLP of the NCEP/NCAR reanalysis data on the long-term time series of monthly mean SLP from 1850 to 2000 given by *Allan and Ansell* [2006] (HadSLP2). The resulting time series of this multivariate regression are for the last 50 years similar to the PCs of the SLP from NCEP/NCAR, but extend back in time as far as 1850. As a last step, the *n* 150 yearlong monthly mean time series are multiplied by the previously obtained respective regression patterns for surface heat flux and wind stress and added together. Thus, by doing so, we reconstructed anomalous surface heat and wind stress for the past 150 years by using long-term SLP data. The resulting forcing time series are finally added to the climatological forcing driving the ocean model.

[12] The same method was applied by *Eden and Jung* [2001] using the NAO index [*Hurrell*, 1995] instead of the leading EOF of SLP to reconstruct the forcing for a very similar ocean model. Note that we found very similar results in the reconstructed forcing time series and in the model simulation using the first leading EOF of SLP or the NAO index [after *Rogers*, 1984] past 1870. Therefore, we refer to the reconstruction using the first leading EOF of HADSLP only as "NAO-related forcing." We will discus the model results of the NAO-related forcing in comparison to simulations driven by reconstructed surface forcing using the first 2 and 4 leading EOFs of HADSLP. To investigate the relative importance of wind stress and heat fluxes both forcing time series were applied individually as well. Note, that anomalous precipitation/evaporation is not included in this model setup. All model experiments which we are discussing below are listed in Table 1. In the latter, positive CO_2 fluxes denote an uptake of CO_2 by the oceans.

3. Validation

3.1. Validating the Mean Simulation

[13] After the 50 year spin-up of the biogeochemical model (150 years for the circulation), the simulated mean CO_2 uptake is on the order of magnitude of 0.25 Pg C/yr which agrees well with the observational estimates of [*Gruber et al.*, 2002]. In our model, there is uptake of CO_2 roughly north of about 30°N with 50 mol C/m^2/yr at maximum in the subpolar gyre region, and release of CO_2 south of 30°N with maximal values in the western tropical Atlantic and the Caribbean Sea. Note, however, the region off the coast of Newfoundland, where a local minimum in CO_2 uptake is modeled related to a well known model bias in the location of the subpolar front [*Eden and Oschlies*, 2006] in that region.

[14] Comparison with the CO_2 flux estimates of *Takahashi et al.* [2002] show in general good agreement with respect to the order of magnitude of the CO2 fluxes and a similar position of the zero line in CO_2 uptake (Figure 1). Note

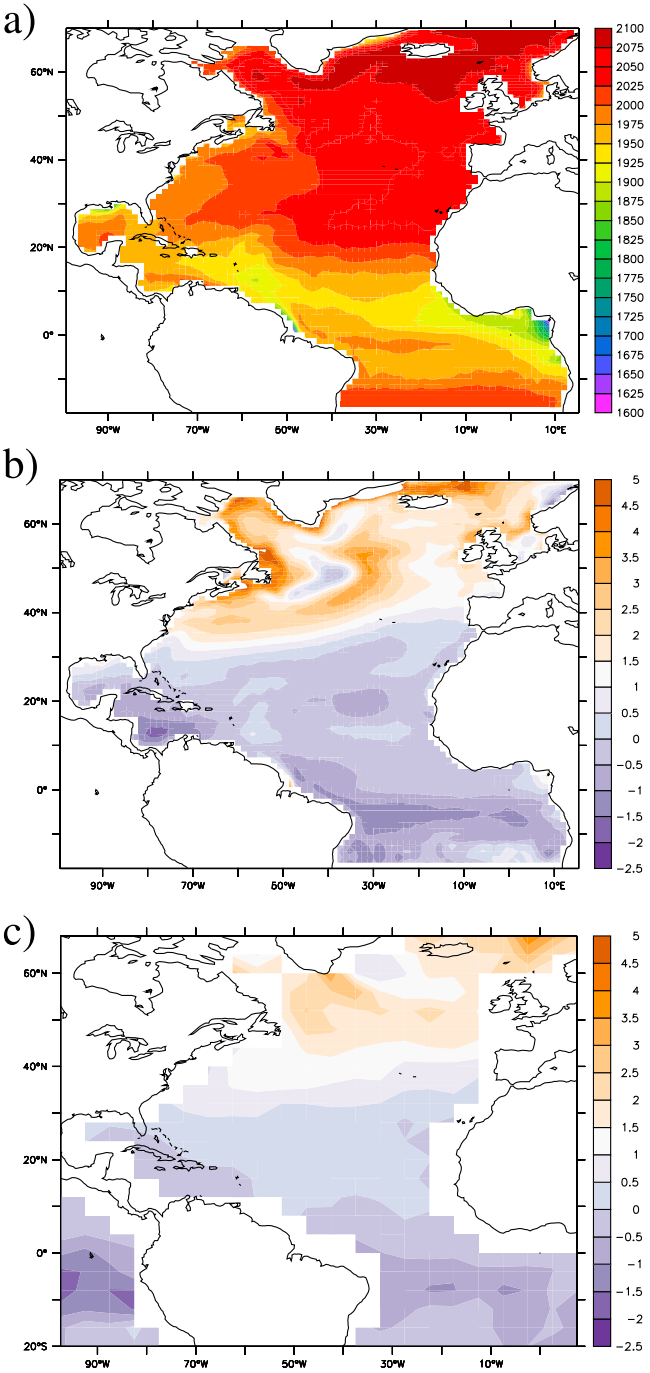

Figure 1. (a) Long-term mean surface DIC concentration in mmol C/m^3 in experiment NAO-FULL. (b) Long-term mean surface CO_2 flux in mol C/m^2/yr for experiment NAO-FULL. Positive values denote oceanic carbon uptake. (c) Estimated CO_2 flux in mol C/m^2/yr from *Takahashi et al.* [2002].

that large differences occur in the high-latitude coastal regions.

[15] Figure 1a shows the concentration of dissolved inorganic carbon (DIC) at the sea surface. In agreement to the surface fluxes and the higher solubility of CO_2 in cold water, the surface DIC content is much higher in high latitudes. Similar results where obtained by *Friedrich et al.* [2006], who used the same model. They find that the general patterns of observational estimates of preindustrial surface concentrations of DIC are generally reproduced by the model. However, some difficulties remain in the eastern equatorial Atlantic and the Amazon river plume where the DIC values are systematically underestimated by the model. Concerning the latter, some influence of the Amazon river might be observed that is not covered by our forcing. *Friedrich et al.* [2006] also showed that the simulated mean annual cycle of pCO_2 near Bermuda agrees closely with a compilation of CO_2 measurements. However, in agreement to previous studies, *Friedrich et al.* [2006] also found that the interannual variability in this region is underestimated by approximately a factor of two, which was related to the lack of mesoscale and submesoscale variability in the simulation.

[16] Given the potential importance of biological processes on the CO_2 fluxes, Figure 2 compares the mean simulated chlorophyll concentration with SeaWIFS observations (1998–2000). Note, that chlorophyll is not a prognostic variable but is diagnosed from phytoplankton assuming a constant ratio 1.59 mg Chl/mmol N. While the magnitude and the large-scale pattern roughly agree, large differences occur in coastal regions where our model fails to resolve relevant processes. Thus, shelf sea processes which were recently investigated by *Thomas et al.* [2004] are not well represented. Also, our non-eddy-resolving ocean model neglects the vertical flux of nutrients induced by the dynamics of mesoscale eddies. The influence of these, however, is still under discussion and different results are presented in the literature [e.g., *McGillicuddy et al.*, 1998; *Oschlies and Garcon*, 2002].

3.2. Validating the Multidecadal Forcing

[17] The monthly reconstructed surface forcing fields gain more and more precision when using an increasing number of PCs by construction. Table 2 shows the explained variances of the reconstructed fields using different numbers of leading SLP modes. We focus here on the winter season (JFM) where the interannual variability of the considered variables is largest (the other seasons are similar as what is discussed below, although with somewhat less explained variance). Using 1 PC for the reconstruction, the explained variance with respect to the surface wintertime heat fluxes of the entire domain in the NCEP/NCAR reanalysis data is 19.8%, while using 4 PCs for the reconstruction the explained variance increases to 47.4%. The reconstruction yields less explained variance in terms of wind stress curl (11.7% and 21.4% explained variance using 1 or 4 PCs, respectively) but more explained variance in terms of the zonal near surface winds (39.7% and 65% explained variance using 1 or 4 PCs, respectively). Similar values of explained variance as for the zonal winds can be found for the meridional near surface winds. The reason for the decreased explained variance of the wind stress curl is most likely related to the increased importance of small-scale features in the curl (by taking the spatial derivatives) compared to the surface winds, which are less well represented in the reconstruction. However, we assume that for our application the small-scale features in the wind stress curl are not important and that the large-scale features of the wind stress curl are sufficiently represented.

[18] Note, that the variance of the NCEP/NCAR surface heat flux and wind stress forcing is better reconstructed in mid and to high latitudes, compared to low latitudes. Table 2 also shows the explained variances for latitudes larger than 30°N, which is significantly higher than for the entire domain. For the subtropical to subpolar surface heat fluxes the reconstruction yields explained variances of 36.3 to 58.0% using 1 or 4 PCs, respectively. A similar relative increase in explained variance holds for surface zonal winds and wind stress curl. The reason for the better performance of the reconstruction toward higher latitudes is because the EOF analysis of the SLP is biased toward variability patterns over the subpolar North Atlantic, while in low latitudes the interannual SLP variability is not as large as for higher latitudes. A method to overcome this limitation of the reconstruction to atmospheric variability in high latitudes would be to restrict the EOF analysis of SLP to low latitudes only, or to use a combination of low- and high-latitude EOFs. However, here we restrict the reconstruction of surface fluxes using the atmospheric variability patterns from high latitudes.

[19] Figure 3 shows the zonally integrated wintertime (JFM) heat flux using 1 PC, 2 PC and 4 PCs for reconstruction in comparison to the wintertime heat flux from the NCEP/NCAR data set. In the subpolar North Atlantic the reconstruction of the surface heat flux covers already the bulk of the interannual variability by using 1 PC. This variability is dominated by a dipole structure over the subtropical to subpolar North Atlantic, which is related to the NAO. Using 2 and 4 PCs for reconstruction, variability patterns which are orthogonal to the leading mode begin to show up, and the total variance of the reconstructed heat flux variability increases to a similar level as in the observations. A similar dipole pattern related to the NAO can be seen in the wind stress curl reconstruction using 1 PC and also a similar appearance of orthogonal patterns related to the higher EOFs (not shown).

4. Results

4.1. Multidecadal Circulation Variability

[20] Figure 4 shows the response of the circulation to the reconstructed forcing in terms of the MOC at the subpolar front. As discussed by *Eden and Jung* [2001] and *Eden and Willebrand* [2001], the interannual to multidecadal variability of the circulation in the high-latitude North Atlantic can be recovered to a large extent by the reconstructed forcing using the leading mode (i.e., the NAO) only. The anomalous strength of the meridional overturning circulation at 48°N is depicted in the overlapping period for the experiments driven with full NCEP forcing (NCEP-FULL) and the reconstructed wind stress and heat flux forcing based on the NAO index (NAO-FULL). The MOC shows very similar decadal variability in both simulations. In particular, the increase of the MOC from the 1970s onward is reproduced in both experiments. In NAO-FULL the trend in the MOC over the recent 50 years can be related to be part of a multidecadal oscillation. Note that since control integrations with climatological forcing for the same time period do

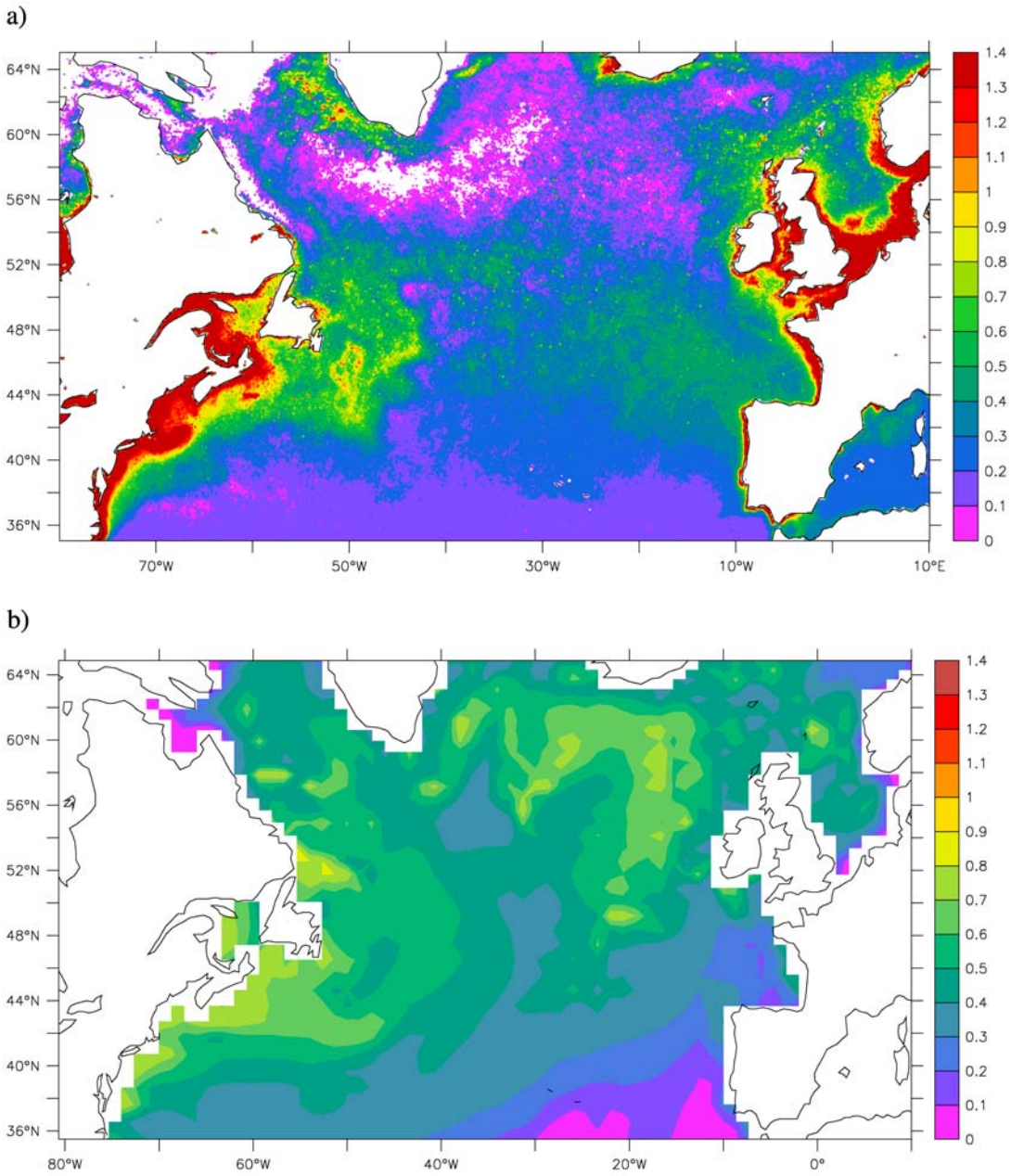

Figure 2. Mean chlorophyll concentration (1998–2000) (mg chl/m^3) (a) as observed by SeaWIFS and (b) as modeled in NAO-FULL (average concentration in the upper 25 m).

Table 2. Explained Variance of the Reconstructed Time Series With Respect to the Wintertime Surface Heat Fluxes, Wind Stress Curl, and Near-Surface Zonal Wind From the NCEP-NCAR Reanalysis Data for the Years 1948–2000[a]

Experiment[b]	Flux[c] (%)	Curl[d] (%)	U[e] (%)	Flux >30°N[f] (%)	Curl >30°N[f] (%)	U >30°N[f] (%)
1-PC	19.8	11.7	39.7	36.3	13.7	45.3
2-PC	35.3	15.0	51.4	41.1	17.4	58.0
3-PC	44.1	19.6	60.9	52.8	22.5	69.0
4-PC	47.4	21.4	65.0	58.0	24.6	74.1

[a]Wintertime is January, February, and March.
[b]Includes numbers of leading modes used for the reconstruction.
[c]Denotes the explained variance for the wintertime surface heat fluxes in the entire model domain.
[d]Denotes the explained variance for the wind stress curl in the entire domain.
[e]Denotes the explained variance for the wintertime zonal wind in the entire model domain.
[f]Denotes the explained variance in the region 30°N to 70°N.

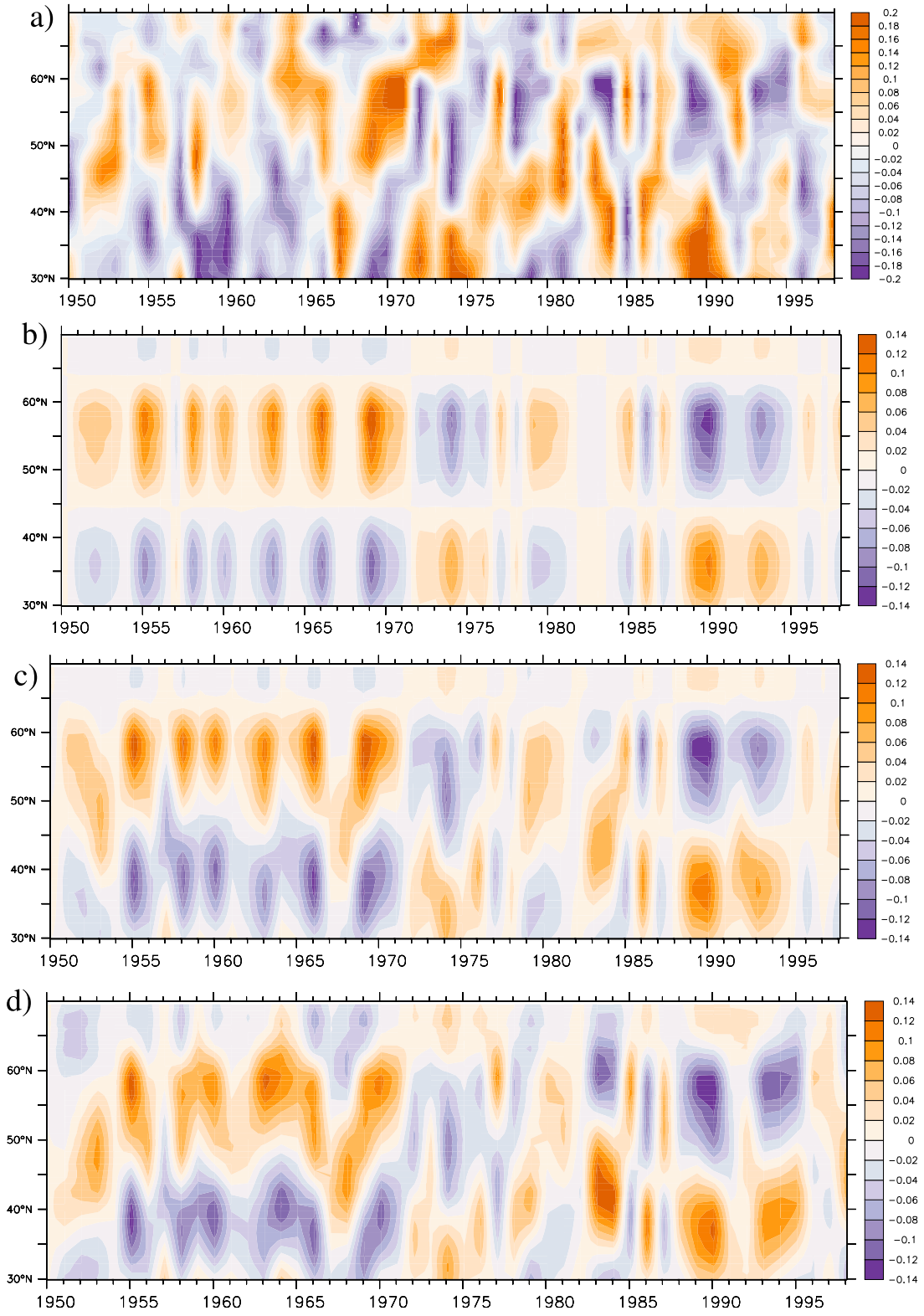

Figure 3. Zonally integrated monthly mean winter (JFM) heat flux forcing (G W/m^2) for the different experiments: (a) full NCEP forcing, (b) the reconstructed forcing by using 1-PC, (c) 2-PC, and (d) 4-PC. The heat flux anomalies are directed from the atmosphere to the ocean.

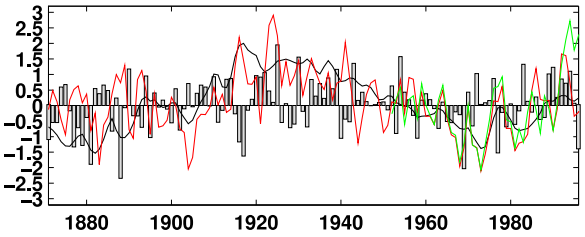

Figure 4. Anomalous strength of the meridional overturning circulation at 48°N at 1000 m depth in Sv in experiment NAO-HEAT (black line), NAO-FULL (red line), and NCEP-FULL (green line). The bars depict the NAO index.

not show that behavior (here, only long-term trends which are orders of magnitude smaller develop; not shown), we conclude that the simulated multidecadal variability in the MOC is driven by the reconstructed forcing time series. It was shown by *Eden and Jung* [2001] that similar multidecadal oscillations with similar relative magnitude show up in the northward heat transport and the horizontal gyre circulation.

[21] Figure 4 also shows that the multidecadal MOC changes are comparable in the experiments driven by anomalous NAO-related heat fluxes (NAO-HEAT) and anomalous NAO-related heat fluxes plus wind stress (NAO-FULL). In fact, it was also found by *Eden and Jung* [2001] that the influence of variability in freshwater flux and wind stress is rather small in this respect, such that the multidecadal changes in the surface heat fluxes are the predominant driver of multidecadal MOC changes. For comparison, the NAO index is depicted in Figure 4 as well, indicating that the multidecadal changes in the surface heat fluxes driving the MOC changes (with a lag of about a decade) are related to multidecadal changes in the observed NAO index. Note that in experiments 2PC-FULL and 4PC-FULL, i.e., using more than the leading model (NAO) for the reconstruction of the surface fluxes, leads to similar multidecadal circulation changes as in NAO-FULL (not shown). We therefore conclude that the reconstruction using the leading atmospheric pattern for reconstructing the forcing is sufficient to generate the bulk of the multidecadal variability in the circulation of the North Atlantic.

4.2. Interannual to Multidecadal Variability in CO_2 Uptake

[22] Since the circulation in the North Atlantic region on multidecadal timescales depends strongly on the NAO index the question arises whether the same holds for the CO_2 fluxes. Thus, we consider the experiment with NAO-related forcing in comparison to the experiments using more than the leading mode for the surface flux reconstruction on both, interannual and multidecadal, timescales. Figure 5 compares the zonally integrated, unfiltered CO_2 fluxes of the experiments with reconstructed forcing (NAO-FULL and 4PC-FULL) with the fluxes of the experiment driven with full NCEP forcing (NCEP-FULL) for the overlapping period 1948–2000. It is obvious that the simulations with reconstructed forcing do not exactly reproduce the flux variability of the reference experiment NCEP-FULL. This is in particular true for the interannual variability, which is not well captured by NAO-FULL. Note that this failure in reproducing the interannual variability by driving the model with NAO-related forcing only is in agreement with the low correlation between NAO and CO_2 uptake of the North Atlantic as reported by previous studies [*McKinley et al.*, 2004; *Raynaud et al.*, 2005]. However, the agreement in terms of the interannual variability of the zonally integrated CO_2 fluxes is getting better when comparing NCEP-FULL and 4PC-FULL. Also the spatial pattern show much more details which are neglected when using the simplified forcing based on the NAO index. However, a part of the variability in the reference experiment is still missing, even in 4PC-FULL.

[23] On longer timescales the ability of the reconstructed forcing to simulate the CO_2 fluxes in agreement with the full NCEP forcing seems to improve: in all experiments a similar interdecadal change, i.e., a trend toward higher CO_2 uptake from the 1970s onward can be noted. In fact, this trend turns out to be part of a multidecadal oscillation. Figure 6 shows the smoothed, basin-wide integrated air-sea CO_2 flux variability north of 20°N for NAO-FULL, 2PC-FULL and 4PC-FULL. All multidecadal model simulations show a similar striking multidecadal variability in CO_2 uptake, regardless of the number of leading modes used for the reconstruction of the surface flux forcing. The magnitude of the simulated multidecadal CO_2 uptake changes is on the order of 0.02 Pg C/yr. Since the multidecadal oscillation shows up in all experiments, the NAO seems to be the dominant factor in determining the changes of the CO_2 flux in the North Atlantic on multidecadal timescales. Note, however, that this is very different on interannual timescales. Increasing the number of leading modes used for the reconstruction clearly leads to better agreement of the interannual air-sea CO_2 flux variability in comparison to the full NCEP/NCAR forcing during the last 50 years. Therefore, more modes than just the NAO are necessary to reconstruct the CO_2 flux variability on interannual timescales and even using the leading 4 modes appears to be insufficient to explain the interannual CO_2 flux variability.

[24] After identifying the NAO as dominant factor in driving the CO_2 flux variability on multidecadal timescales, the question arises whether the NAO influences the CO_2 fluxes through heat fluxes or wind stress or both. Using a very similar model, *Friedrich et al.* [2006] found that the wind stress is the dominant factor driving interannual CO_2 flux variability in the North Atlantic, while surface heat fluxes and other surface forcing does not play an important role. The same results are obtained in the present study. However, for the multidecadal CO_2 flux variability in the North Atlantic the surface heat flux variability related to the NAO appears to be of similar importance as the multidecadal wind stress changes. Figure 7 shows the basin-wide integrated CO_2 flux variability for experiments NAO-FULL in comparison with NAO-HEAT and NAO-WIND, in which the model was forced only with NAO-related heat flux or wind stress variability, respectively. Both multidecadal wind stress and heat flux forcing are driving similar multidecadal oscillations in the CO_2 uptake.

4.3. Mechanisms Driving the Multidecadal Variability in CO_2 Uptake

[25] We next discuss the drivers of the multidecadal variability of the CO_2 fluxes more in detail. The possible driving mechanisms of the variability in the CO_2 fluxes are

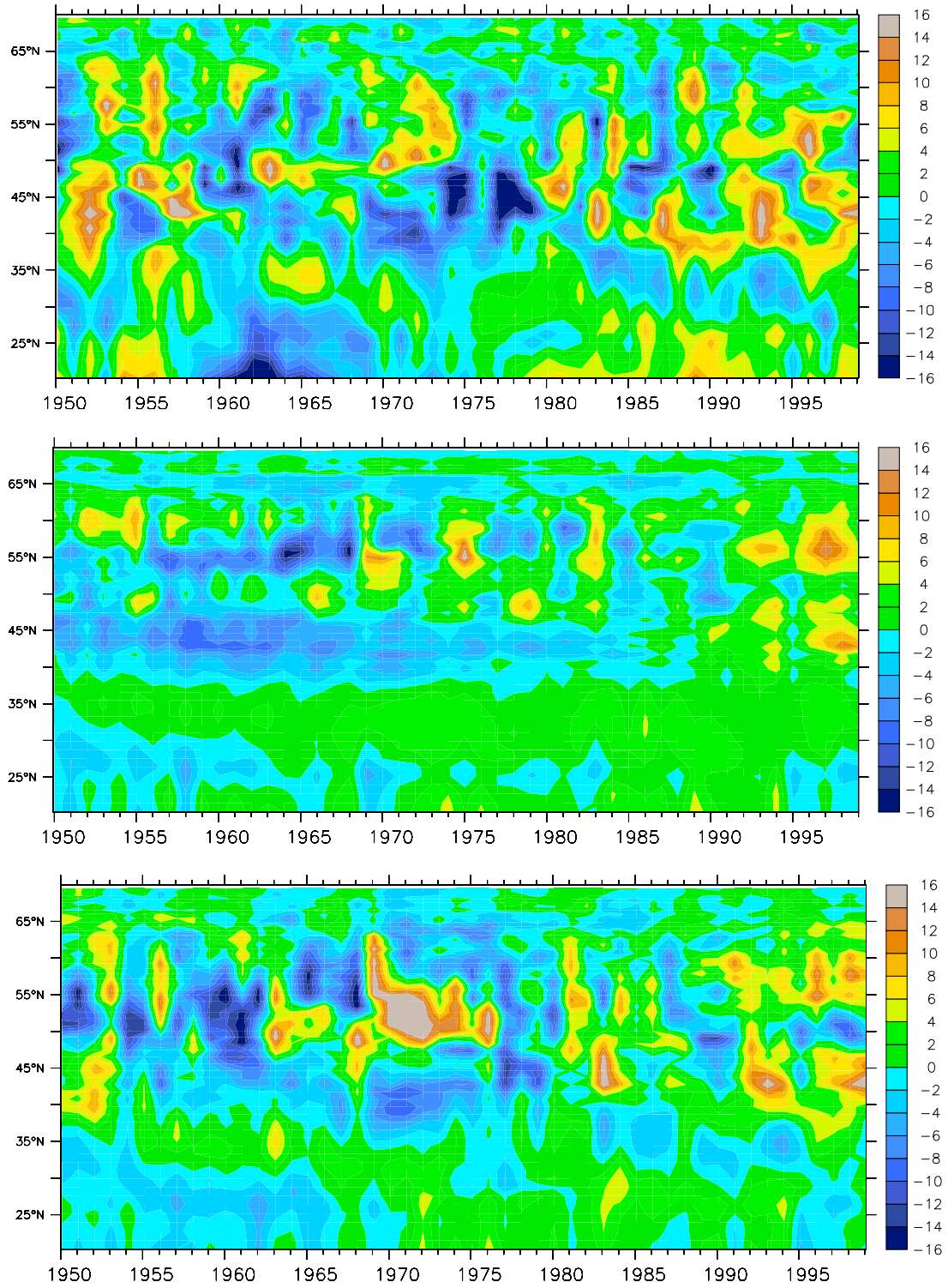

Figure 5. Zonally integrated CO_2 flux changes in (top) NCEP-FULL, (middle) NAO-FULL, and (bottom) 4PC-FULL (tC/m/yr). Positive fluxes denote CO_2 uptake of the ocean.

biological processes, surface fluxes and physical transport processes.

[26] First, we explore the role of the biological component (neglecting alkalinity here which is treated in the context of salinity changes). The multidecadal variability in the surface chlorophyll is, in agreement with [*Oschlies*, 2001], largest in the subtropics and strongly related to NAO fluctuations (not shown). However, the integrated multidecadal variability of the chlorophyll concentration in the euphotic zone is rather small in our model (basin-wide 1–2 percentage) and accordingly, our estimates of the biological pump contributing to the anomalous CO_2 fluxes are more than 1 order of magnitude

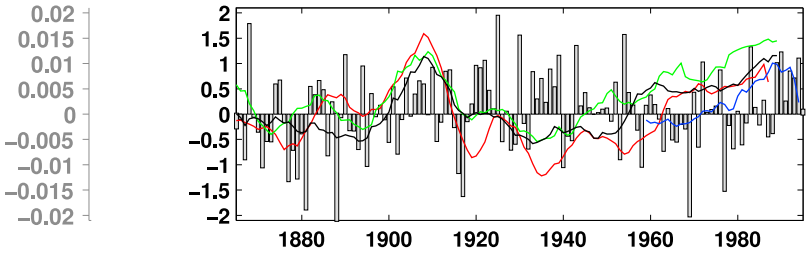

Figure 6. Smoothed (10 year running mean) basin-wide air-sea CO_2 flux anomalies integrated over the North Atlantic north of 20°N for different experiments with reconstructed heat flux and wind stress forcing in Pg C/yr. Different leading modes of the SLP data are used for reconstruction. The red line shows the CO_2 fluxes when only the first leading mode is used, for the green line two leading modes are used, and for the experiment corresponding to the black line four modes are applied. The blue line depicts the experiment with full NCEP forcing which is only available for the last 50 years. The bars depict the NAO index. The corresponding y axis is drawn directly to Figure 6, while the second gray axis refers to the fluxes.

smaller than the simulated multidecadal flux variability. Note, however, that we are using a rather simplified biological model and furthermore the importance of the biological pump might change under global warming conditions. Given the weak influence of the biological pump on the multidecadal variability in our model, we focus on the physical processes in the following.

[27] Since anomalous dilution or concentration effects are not included into our model setup, the bulk of the pCO_2 variability can be attributed to physical transport processes. As shown before, the NAO is the dominate factor for the basin-wide CO_2 fluxes, while a direct linear connection with the NAO index is not obvious (Figure 6). Thus, our aim is now to investigate the underlying mechanisms. For this purpose, we compute the difference between the periods 1920–1940 and 1960–1980 based on the integration NAO-FULL. The periods are chosen to represent phases with anomalous high and low NAO index and the difference thus provides a measure of the overall amplitude of the variability from a high to low NAO index. Figure 8a shows the differences in the CO_2 fluxes between both periods. The main variations occur in the north western part of the North Atlantic. In the Labrador Sea and off Newfoundland the positive NAO phase is connected with a negative CO_2 flux anomaly while a positive anomaly occurs in the vicinity of the North Atlantic current. Thus, both anomalies compensate for the most part when considering the integrated basin-wide fluxes. Similar pattern are obtained when using different periods of anomalous high and low NAO index. Figure 8b shows the same differences as before but for modeled pCO_2. In agreement with Figure 8a the fluxes are high where pCO_2 is low and vice versa. Considering the CO_2 flux differences for the experiment NAO-HEAT (Figure 8c) and NAO-WIND (Figure 8d) reveals that the negative flux anomaly is mainly wind driven while the positive anomaly is to a large degree due to surface heat flux forcing.

[28] Since in our model pCO_2 is a function of surface salinity, temperature and DIC content only, we investigate these pattern more in detail. Note, that in our model changes in alkalinity are included in salinity changes and a large part of the influence of salinity can be attributed to changes in alkalinity. The exact formulation is given by *Eden and*

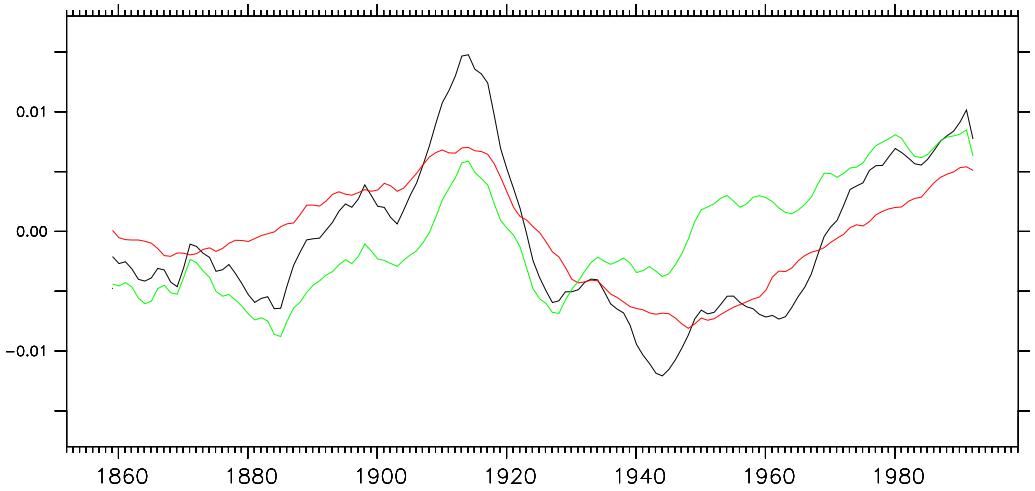

Figure 7. Smoothed (15 year running mean) mean air-sea CO_2 flux anomalies averaged over the North Atlantic for the experiments NAO-FULL (black line), NAO-HEAT (red line), and NAO-WIND (green line) (Pg C/yr).

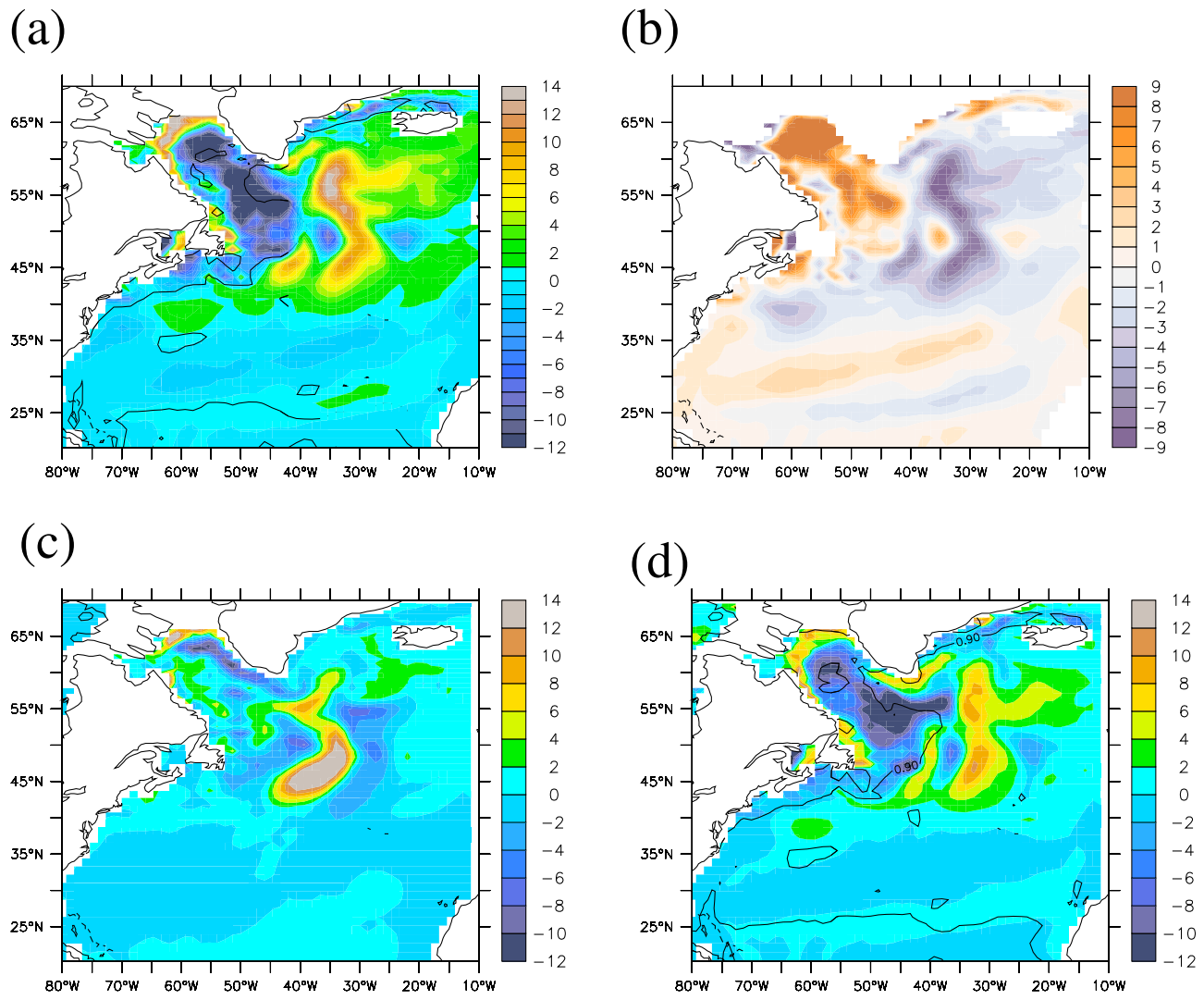

Figure 8. (a) Difference of the simulated CO_2 fluxes between the periods 1920–1940 and 1960–1980 ($g/m^2/yr$) based on the experiment NAO-FULL. The black line marks the 0.9 level of the correlation between DIC content and salinity. The periods are chosen to represent the difference between a period with anomalous high versus a period with anomalous low NAO index. (b) Corresponding difference in the simulated sea surface pCO_2 (ppm). (c) As in Figure 8a for the experiment NAO-HEAT. (d) As in Figure 8a for the experiment NAO-WIND.

Oschlies [2006] ($ALK = -0.5487S^3 + 59.919S^2 - 21223.3S + 26722$ ($mmol/m^3$)). They also estimated the ability of the single quantities to influence pCO_2 and found typical values of 10 ppm/K for temperature, −60 ppm/psu for salinity (including alkalinity) and 1 ppm/mmol/m^3 for DIC. This decomposition is not valid in the presence of sea ice and thus we do not discuss the ice edge more in detail here. Figure 9 shows the anomalies in temperature, salinity and DIC content corresponding to the time periods chosen in Figure 8. All quantities exhibit positive anomalies in the Labrador Sea and off Newfoundland during high NAO phases. Those are especially pronounced for salinity and DIC content. Since both quantities have an opposite effect on pCO_2, the anomalies compensate partly in their effect. Remarkably, the western pattern in the Labrador Sea and off Newfoundland are much less pronounced in the experiment NAO-HEAT with an order of magnitude of approximately 25% compared to NAO-FULL (Figures 8c and 8d). We can conclude that this pattern is largely wind driven. Further to the east, the temperature anomaly gets stronger and the anomaly of DIC content changes sign. The individual influences of surface salinity and DIC content are much smaller here but their effects on pCO_2 add instead of compensating. All anomalies in this region are almost equally pronounced in the experiment NAO-HEAT compared to NAO-FULL and are thus mainly heat flux driven.

[29] Since salinity and DIC content vary in phase in the western part of the area of interest while they show an opposite behavior further to the east, we might separate both regions by calculating the spatial correlation between surface salinity and DIC content. The (significant) 0.9 level is drawn by a thick black line in Figure 8a. The region to the

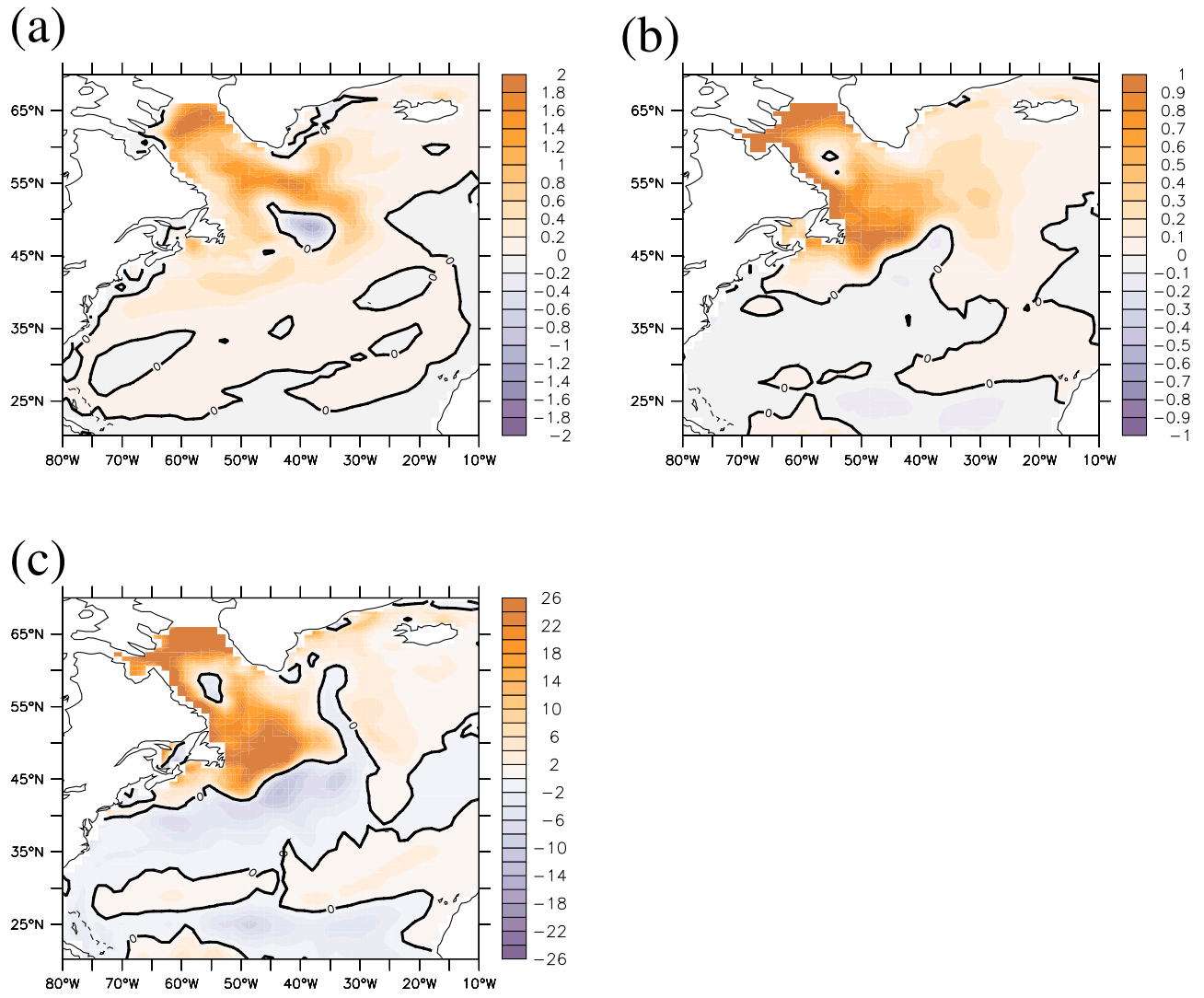

Figure 9. Difference between the periods 1920–1940 and 1960–1980 based on the experiment NAO-FULL of (a) temperature in K, (b) salinity in psu, and (c) DIC in mol/m^3.

left of this line is attributed to region HC (high correlation) and the region to the right of this line to region LC (low correlation) in the following text. In region LC the correlations are mainly negative or very small otherwise. Thus, the mechanisms leading to the CO_2 flux anomalies in region HC and LC are very different. The region LC shows large similarities with the multidecadal temperature anomalies in connection with NAO-driven MOC and gyre changes reported by *Eden and Jung* [2001] who obtain northward propagating, intensifying temperature anomalies during high and low NAO phases. Figure 10 shows similar pattern for surface salinity and DIC content during consecutive 5 year periods from 1950 to 1980. Here, the pattern are depicted for the integration NAO-HEAT. In NAO-FULL the pattern are basically the same but here they are harder to distinguish from anomalies in the region HC. Considering the zonally integrated transport anomalies in the integration NAO-FULL (Figure 11) shows a clear NAO/MOC-related northward transport of heat, salt and DIC with a negative correlation between DIC and salinity.

[30] The second regime, HC, is convective instead of advective as LC. Here, the anomalous high wind speeds during high NAO phases (as depicted in Figure 9) lead to a considerable deepening of the mixed layer and thus water from below is mixed into the mixed layer. As an example, Figure 12 shows the mean mixed layer depth from 1920 to 1940 (equal to high NAO phase) in comparison to 1960–1980 (equal to low NAO phase) overlayed on mean temperature, salinity and DIC content. Since the deeper layers contain as well more salt as DIC both quantities vary in phase in dependence of the mixed layer depth (Figures 12b and 12c) while the temperature gradient is small in the region of interest (Figure 12a). The strong connection between mixed layer depth and surface salinity and DIC content off Newfoundland (48°N to 52°N and 50°W to 40°W) can also be seen in Figure 12d.

[31] Summing up, all anomalies influencing the CO_2 fluxes depend strongly on the NAO index. The regime HC is much stronger in the wind driven integration (NAO-WIND) while LC is much more pronounced in the heat flux driven

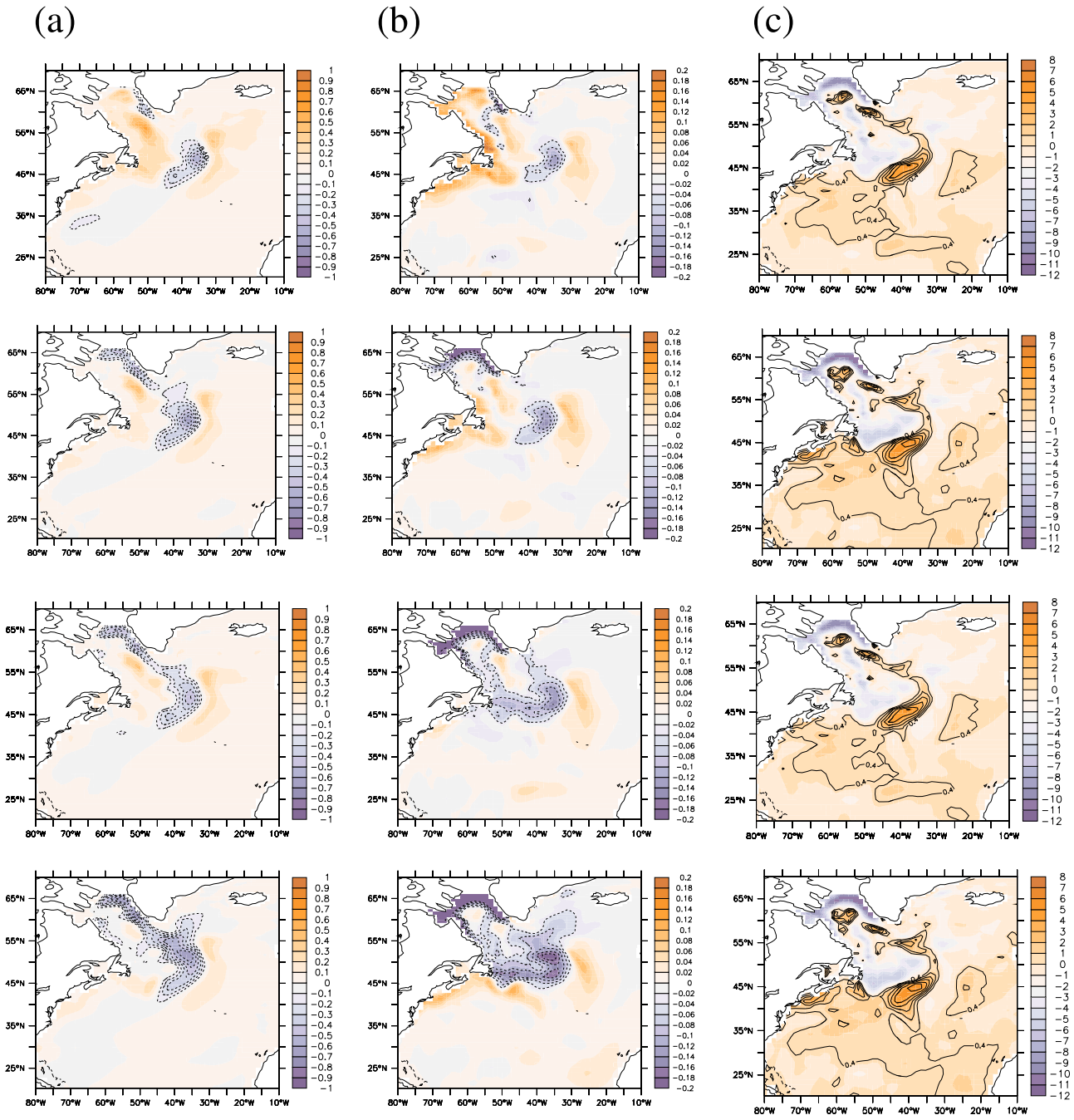

Figure 10. (a) Temperature in K, (b) salinity in psu, and (c) DIC anomalies in mol/m^3 during the development of a low NAO phase during consecutive 5 year periods (1955–1974) based on the model simulation NAO-HEAT.

experiment (NAO-HEAT). Figure 13 shows the time behavior of both regimes. Considering the basin-wide fluxes the regime LC is more pronounced by approximately factor 2. It leads to positive flux anomalies responding with a time lag of 10–20 years. The sign of the regime HC is opposite while the response on NAO changes is instantaneous.

5. Summary and Discussion

[32] *McKinley et al.* [2004] analyzed an off-line model exploring the relative importance of the CO_2 uptake of the tropical Pacific and the North Atlantic Ocean on interannual timescales (a simulation in which flow fields and diffusivities are archived which can then be applied afterward to any passive biogeochemical tracer). They found for the air-sea CO_2 flux variability in their model simulation no significant contribution by the North Atlantic, consistent with the previous carbon cycle simulations. They argued that a cancelation between convectively driven CO_2 changes and changes in biological carbon drawdown might be responsible. The same reasons are assumed to be responsible

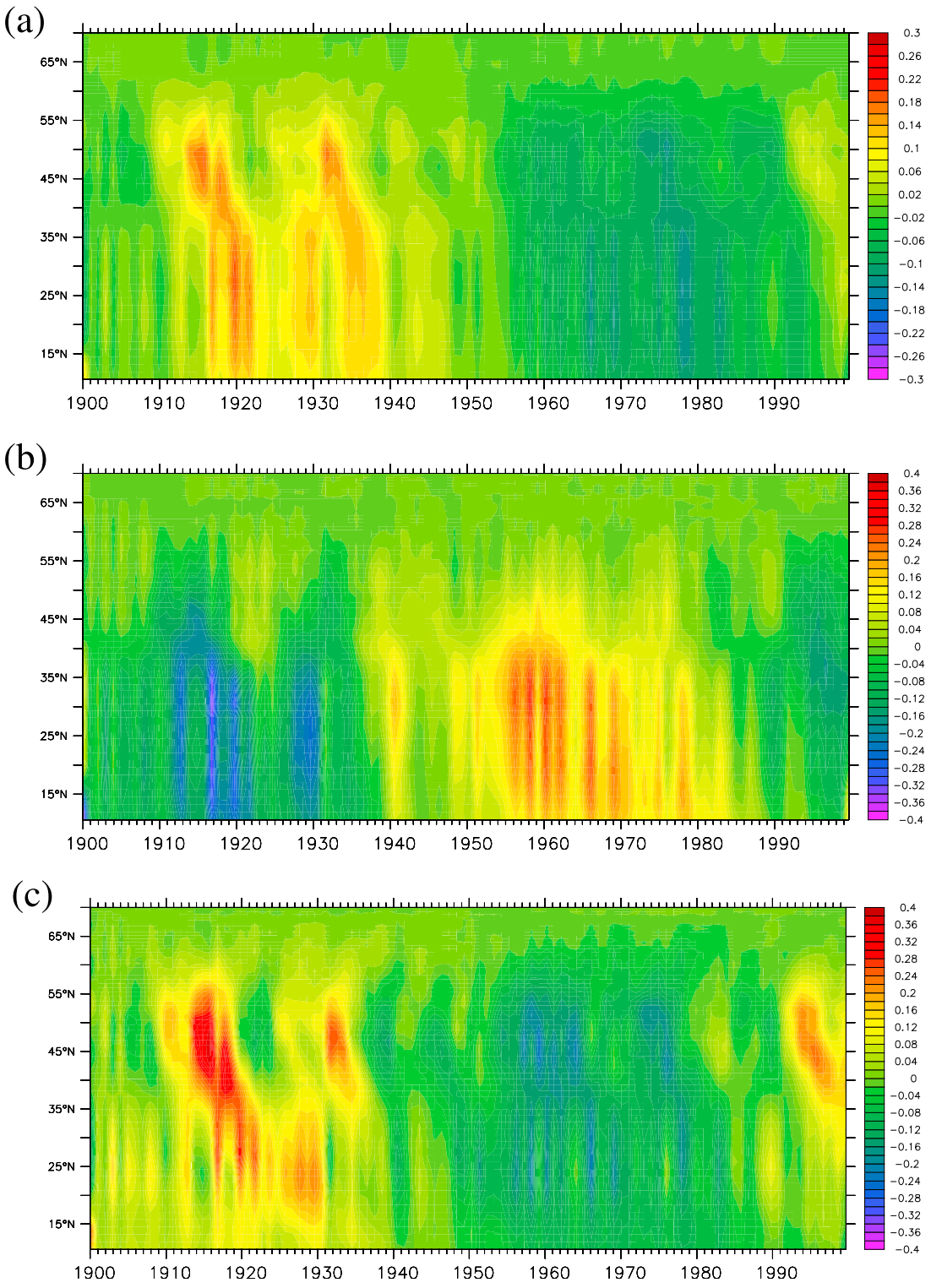

Figure 11. (a) Anomalous northward heat transport in PW considering the experiment NAO-FULL, (b) anomalous northward transport of DIC (mol/m^3*10^{-13}), and (c) anomalous northward salt transport.

for the weak connection between CO_2 fluxes and the NAO index.

[33] Also in our model, the connection between the NAO index and basin-wide CO_2 fluxes is rather weak on interannual timescales while the interannual variability is somewhat stronger than in the work of *McKinley et al.* [2004]. On the multidecadal timescales considered in our study, however, the mechanisms change and the NAO gains more influence by driving changes in the ocean circulation which were already reported by *Eden and Jung* [2001] and through

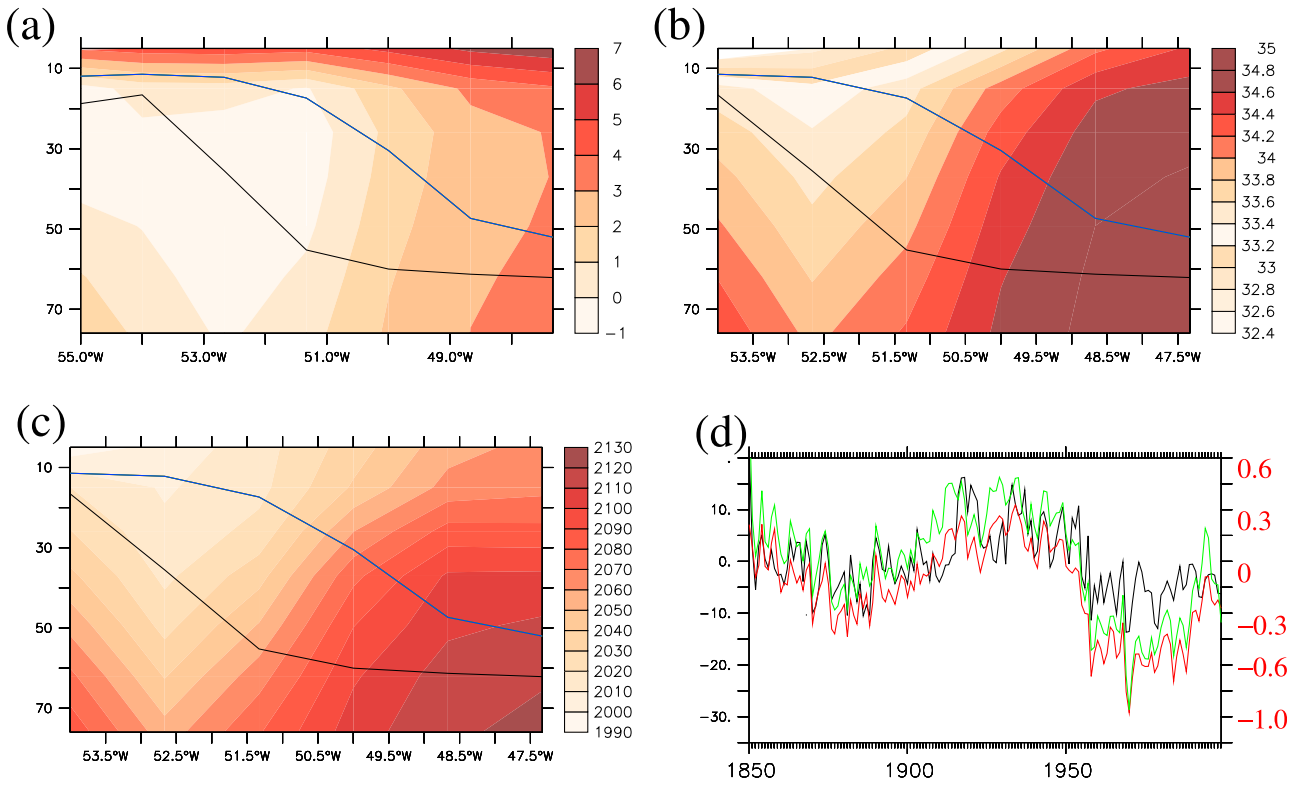

Figure 12. (a) Temperature section in K at 50°N including the mean mixed layer depth for the periods 1920–1940 (black line) and 1960–1980 (blue line) considering the experiment NAO-FULL. The mixed layer depth is defined as the location of a vertical density change of more than 0.01 kg/m^3 compared to the surface layer. (b) Salinity in psu at 50°N including the mean mixed layer depth for the periods 1920–1940 (black line) and 1960–1980 (blue line). (c) DIC content in mol/m^3 at 50°N including the mean mixed layer depth for the periods 1920–1940 (black line) and 1960–1980 (blue line). (d) Anomalous mixed layer depth averaged between 48°N to 52°N and 50°W to 40°W (black line) in comparison to anomalous surface salinity in psu (red line) and DIC content in mol/m^3 (green line).

faster, convective processes off Newfoundland and in the Labrador Sea. This influence of the NAO is to due to both the anomalous heat fluxes and wind stress associated with the NAO. In combination this impacts on temperature and salinity, as well as DIC content which in turn affect the CO_2 fluxes. The role of the biological pump is of minor importance in our simulations.

[34] Since our reconstruction ends in 2000 and the atmospheric CO_2 conditions are set to preindustrial values, a direct comparison with recent observations is not possible. However, in order to asses our coupled biogeochemical/circulation model we integrated an additional simulation driven with full NCEP forcing (NCEP-FULL) which shows a drop in CO_2 uptake over the last years (Figure 14). This is

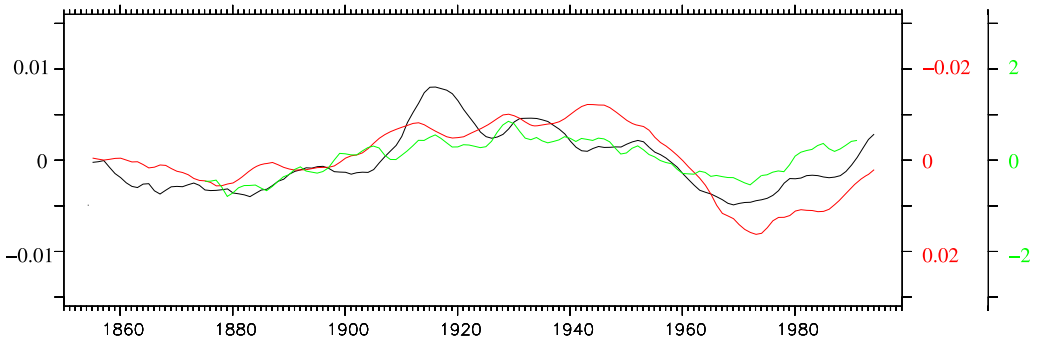

Figure 13. Smoothed (10 year running mean) basin-wide air-sea CO_2 flux anomalies integrated over the North Atlantic north of 20°N for the convective regime (HC, red line) and the advective regime (LC, black line) in Pg C/yr. Note, the different axis for HC and LC. The green line depicts the NAO index (20 year running mean) for comparison.

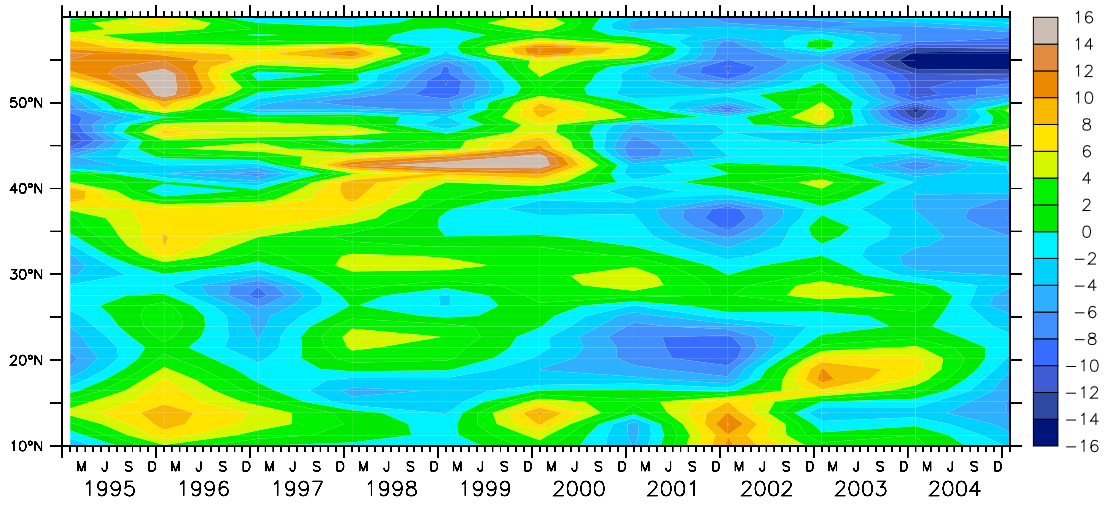

Figure 14. Zonally integrated CO_2 flux (tC/m/yr) over the last decade of the simulation NCEP-FULL.

in line with our previous considerations due to the recent drop of the NAO index and these findings agree well with those of *Lefèvre et al.* [2004] and *Corbiere et al.* [2007] who report, based on observations, a decrease in CO_2 uptake of the subpolar North Atlantic over the last decades. Further, these authors suggest that this is closely related to the NAO index. A similar suggestion is given by *Schuster and Watson* [2007] who evaluated ship measurements.

[35] **Acknowledgments.** This study was supported by the German BMBF. The model integrations have been performed on a NEX-SX8 at the University Kiel and on a NEC-SX6 at the Deutsches Klimarechenzentrum (DKRZ), Hamburg.

References

Allan, R., and T. Ansell (2006), A new globally complete monthly historical gridded mean sea level pressure dataset (HadSLP2): 1850–2004, *J. Clim.*, *19*(22), 5816–5842.

Barnier, B., L. Siefridt, and P. Marchesiello (1995), Thermal forcing for a global ocean circulation model using a three year climatology of ECMWF analysis, *J. Mar. Syst.*, *6*, 363–380.

Boyer, T. P., and S. Levitus (1997), Objective analyses of temperature and salinity for the world ocean on a 1/4 degree grid, *NOAA Atlas NESDIS 11*, U.S. Gov. Print. Off., Washington, D. C.

Cayan, D. R. (1992), Latent and sensible heat flux anomalies over the northern oceans: The connection to monthly atmospheric circulation, *J. Clim.*, *5*, 354–369.

Conway, T. J., P. P. Tans, L. S. Waterman, K. K. Thoning, D. R. Kitzis, K. A. Masarie, and N. Zhang (1994), Evidence for interannual variability of the carbon cycle from the National Oceanic and Atmospheric Administration/Climate Monitoring and Diagnostics Laboratory global air sampling network, *J. Geophys. Res.*, *99*(D11), 22,831–22,856.

Corbiere, A., N. Metzl, G. Reverdin, C. Brunet, and T. Takahashi (2007), Interannual and decadal variability of the oceanic carbon sink in the North Atlantic subpolar gyre, *Tellus, Ser. B*, *59*, 168–178.

Cox, M. D. (1987), Isopycnal diffusion in a z-coordinate ocean model, *Ocean Modell.*, *74*, 1–5.

Eden, C., and T. Jung (2001), North Atlantic interdecadal variability: Oceanic response to the North Atlantic oscillation (1865–1997), *J. Clim.*, *14*(5), 676–691.

Eden, C., and C. Oschlies (2006), Adiabatic reduction of circulation-related CO_2 air-sea flux biases in North Atlantic carbon-cycle models, *Global Biogeochem. Cycles*, *20*, GB2008, doi:10.1029/2005GB002521.

Eden, C., and J. Willebrand (2001), Mechanism of interannual to decadal variability of the North Atlantic circulation, *J. Clim.*, *14*(10), 2266–2280.

Friedrich, T., A. Oschlies, and C. Eden (2006), Role of wind stress and heat fluxes in generating interannual to decadal variability of air-sea CO_2 and O_2 fluxes in a North Atlantic model, *Geophys. Res. Lett.*, *33*, L21S04, doi:10.1029/2006GL026538.

Gaspar, P., Y. Gregoris, and J.-M. Lefevre (1990), A simple eddy kinetic energy model for simulations of the oceanic vertical mixing: Tests at station PAPA and Long-Term Upper Ocean Study site, *J. Geophys. Res.*, *95*, 16,179–16,193.

Gent, P. R., and J. C. McWilliams (1990), Isopycnal mixing in ocean circulation models, *J. Phys. Oceanogr.*, *20*, 150–155.

Gruber, N., C. Keeling, and N. Bates (2002), Interannual variability in the North Atlantic Ocean carbon sink, *Science*, *298*(5602), 2374.

Haney, R. L. (1971), Surface thermal boundary condition for ocean circulation models, *J. Phys. Oceanogr.*, *1*, 79–93.

Hurrell, J., Y. Kushnir, G. Ottersen, and M. Visbeck (2003), An overview of the North Atlantic Oscillation, in *The North Atlantic Oscillation: Climate Significance and Environmental Impact*, *Geophys. Monogr. Ser.*, vol. 134, pp. 1–35, AGU, Washington, D. C.

Hurrell, J. W. (1995), Decadal trends in the North Atlantic Oscillation: Regional temperatures and precipitation, *Science*, *269*, 676–679.

Kalnay, E., et al. (1996), The NCEP/NCAR 40-years reanalysis project, *Bull. Am. Meteorol. Soc.*, *77*, 437–471.

Lefèvre, N., A. Watson, A. Olsen, A. Ríos, F. Pérez, and T. Johannessen (2004), A decrease in the sink for atmospheric CO_2 in the North Atlantic, *Geophys. Res. Lett.*, *31*, L07306, doi:10.1029/2003GL018957.

LeQuere, C., J. C. Orr, P. Monfray, O. Aumont, and G. Madec (2000), Interannual variability of the oceanic sink of CO_2 from 1979 to 1997, *Global Biogeochem. Cycles*, *14*, 1247–1265.

McGillicuddy, D. J. J., A. R. Robinson, D. Siegel, H. Jannasch, R. Johnson, T. Dickey, J. McNeil, A. Michaels, and A. Knap (1998), Influence of mesoscale eddies on new production in the Saragosso Sea, *Nature*, *394*, 263–265.

McKinley, G., M. Follows, and J. Marshall (2004), Mechanisms of air-sea CO_2 flux variability in the equatorial Pacific and the North Atlantic, *Global Biogeochem. Cycles*, *18*, GB2011, doi:10.1029/2003GB002179.

Obata, A., and Y. Kitamura (2003), Interannual variability of the sea-air exchange of CO_2 from 1961 to 1998 simulated with a global ocean circulation-biogeochemistry model, *J. Geophys. Res.*, *108*(C11), 3337, doi:10.1029/2001JC001088.

Oschlies, A. (2001), NAO-induced long-term changes in the nutrient supply in the surface waters of the North Atlantic, *Geophys. Res. Lett.*, *28*, 1751–1754.

Oschlies, A., and V. Garcon (1999), An eddy-permitting coupled physical-biological model of the North Atlantic: 1. Sensitivity to advection numerics and mixed layer physics, *Global Biogeochem. Cycles*, *13*, 135–160.

Oschlies, A., and V. Garcon (2002), Improved representation of upper ocean dynamics and mixed layer depths in a model of the North Atlantic on switching from eddy-permitting to eddy-resolving grid resolution, *J. Phys. Oceanogr.*, *32*, 2277–2298.

Pacanowski, R. C. (1995), MOM 2 documentation, user's guide and reference manual, technical report, Ocean Group, Geophys. Fluid Dyn. Lab., Princeton, N. J.

Raynaud, S., O. Aumont, K. Rodgers, P. Yiou, and J. Orr (2005), Interannual-to-decadal variability of North Atlantic air-sea CO_2 fluxes, *Ocean Sci.*, *2*, 437–472.

Rogers, J. (1984), The association between the North Atlantic Oscillation and the Southern Oscillation in the Northern Hemisphere, *Mon. Weather Rev.*, *112*(10), 1999–2015.

Sabine, C., et al. (2004), The oceanic sink for anthropogenic CO_2, *Science*, *305*(5682), 367–371.

Schuster, U., and A. J. Watson (2007), A variable and decreasing sink for atmospheric CO_2 in the North Atlantic, *J. Geophys. Res.*, *112*, C11006, doi:10.1029/2006JC003941.

Takahashi, T., et al. (2002), Global sea-air CO_2 flux based on climatological surface ocean pCO_2, and seasonal biological and temperature effects, *Deep Sea Res., Part II*, *49*(9–10), 1601–1622.

Thomas, H., Y. Bozec, K. Elkalay, and H. J. W. de Baar (2004), Enhanced open ocean storage of CO_2 from shelf sea pumping, *Science*, *304*, 1005–1008.

Wanninkhof, R. (1992), Relationship between gas exchange and wind speed over the ocean, *J. Geophys. Res.*, *97*, 7373–7381.

Watson, A. J., et al. (2009), Tracking the variable North Atlantic sink for atmospheric CO_2, *Science*, *326*, 1391–1393, doi:10.1126/science.1177394.

Wetzel, P., A. Winguth, and E. Maier-Reimer (2005), Sea-to-air CO_2 flux from 1948 to 2003: A model study, *Global Biogeochem. Cycles*, *19*, GB2005, doi:10.1029/2004GB002339.

C. Eden, Leibniz Institute of Marine Sciences at University of Kiel (IFM-GEOMAR), Düsternbrooker Weg 20, D-24105 Kiel, Germany.

U. Löptien, Swedish Meteorological and Hydrological Institute, Folkborgsvägen 1, SE-601 76 Norrköping, Sweden. (uloeptien@ifm-geomar.de)